Biomaterials 31 (2010) 1093–1103

Contents lists available at ScienceDirect

Biomaterials

journal homepage: www.elsevier.com/locate/biomaterials

Corrosion of, and cellular responses to Mg–Zn–Ca bulk metallic glasses

Xuenan Gu [a], Yufeng Zheng [a,b,*], Shengping Zhong [b], Tingfei Xi [b], Junqiang Wang [c], Weihua Wang [c]

[a] State Key Laboratory for Turbulence and Complex System and Department of Advanced Materials and Nanotechnology, College of Engineering, Peking University, No. 5, Yi-He-Yuan Road, Beijing 100871, China
[b] Center for Biomedical Materials and Tissue Engineering, Academy for Advanced Interdisciplinary Studies, Peking University, Beijing 100871, China
[c] Institute of Physics, Chinese Academy of Science, Beijing 100080, China

ARTICLE INFO

Article history:
Received 26 September 2009
Accepted 3 November 2009
Available online 24 November 2009

Keywords:
Magnesium alloy
Bulk metallic glass
Mechanical property
Corrosion
Cytotoxicity

ABSTRACT

Mg–Zn–Ca bulk metallic glass with different compositions (Mg66Zn30Ca4 and Mg70Zn25Ca5) have been prepared for this study and their feasibility as biodegradable metallic materials have been evaluated by the microstructural, surface analysis, mechanical testing, corrosion and cytotoxicity tests. It was found that the Mg66Zn30Ca4 sample presents a more uniform corrosion morphology than as-rolled pure Mg and Mg70Zn25Ca5 samples, with much smaller micro-scale uniformly distributed pores beneath the corrosion product layer. The corrosion products were identified to be $Mg(OH)_2$ and $Zn(OH)_2$, and a uniform corrosion mechanism is proposed. Both indirect cytotoxicity and direct cell culture experiments were carried out using L929 and MG63 cell lines. The results show higher cell viabilities for Mg–Zn–Ca extracts than that for as-rolled pure Mg. In addition, L929 and MG63 cells were found to adhere and proliferate on the surface of Mg66Zn30Ca4 sample.

1. Introduction

Magnesium alloys have attracted considerable attention as potential implant materials in recent years [1–5]. This interest in magnesium alloys has been particularly motivated by their good mechanical properties, biocompatibilities and biodegradation properties [6]. One group of magnesium alloys, containing the essential elements Zn and Ca for humans, have been especially studied with reference to biosafety and biocompatibility of released alloying elements [3–5,7]. For example, Zhang et al. [7] reported that an Mg–Zn alloy had high tensile strength (279.5 MPa) and no adverse effect had been caused by the zinc released. Our study indicated that Mg–1Ca alloy degraded gradually within bone at the corrosion rate of 2.28 mg/mm^2/yr and an enhanced bone formation was visible around implanted pins [5].

However, the practical usage of biodegradable magnesium alloys faces some challenges. Firstly, a much higher inherent strength will be required since their strength would deteriorate gradually during the corrosion/degradation process [7]. Zhang et al. [7] reported that the bending strength of Mg–Zn alloy decreased fast at the initial corrosion stage (from about 625 MPa to 390 MPa with about 6% loss of weight). Secondly, magnesium alloys usually suffer from non-uniform corrosion. Pitting corrosion is the typical corrosion mode of Mg alloys even in neutral or alkaline salt solutions [8] and the pits tend to spread laterally resulting in the disintegration of the alloys during the corrosion period [5,9]. Witte et al. [2] indicated that LAE442 and AZ91D alloys showed irregular, uneven surface after 18 weeks implantation in guinea pigs femora. Our previous study on Mg–1Ca alloy also showed non-uniform corrosion properties within bone [5]. Moreover, pitting corrosion, resulting in the surface defects, will also lead to the fast loss of the strength of magnesium alloys. Thirdly, current magnesium alloys have corrosion/degradation rates under physiological conditions that are too fast and indeed faster than that of bone healing rates [5,6,10]. At the same time, the release of hydrogen and localized alkalization caused by the fast corrosion [1,11] may also be deleterious to the surrounding tissues. Therefore, it is very important to explore new kinds of magnesium-based biomaterials with good mechanical properties, low corrosion rates as well as the uniform corrosion properties in order to be applied clinically.

Magnesium-based bulk metallic glasses are attractive due to their single-phase, chemically homogeneous alloy system and the absence of second phases [12–14] which may improve the mechanical properties and corrosion resistance and also result in more uniform corrosion properties. Various Mg-based glasses have

* Corresponding author. State Key Laboratory for Turbulence and Complex System and Department of Advanced Materials and Nanotechnology, College of Engineering, Peking University, No. 5, Yi-He-Yuan Road, Beijing 100871, China. Tel./fax: +86 10 6276 7411.
E-mail address: yfzheng@pku.edu.cn (Y. Zheng).

0142-9612/$ – see front matter © 2009 Elsevier Ltd. All rights reserved.
doi:10.1016/j.biomaterials.2009.11.015

been developed, including Mg–Cu–Y, Mg–Ni–Y, Mg–Cu–Gd and Mg–Zn–Ca [12]. Among them, Mg–Zn–Ca exhibits a high specific strength (σ_f/ρ) of 250–300 MPa cm^3/g [15], which is about 40% higher than that of conventional crystalline Mg alloys (about 220 and 176 MPa cm^3/g for diecasting AZ91D and WE43 [16]). With the physiologically compatible alloying element Zn and Ca [17,18], Mg–Zn–Ca glass might be an appropriate choice for magnesium-based biodegradable materials. In this study, Mg-based glasses with good glass forming ability (GFA) and different Mg content, Mg66Zn30Ca4 and Mg70Zn25Ca5 glasses, were fabricated, and their corrosion properties and the indirect and direct cytocompatibilities were studied.

2. Experimental

2.1. Materials preparation and characterization

A mixture of pure elements (>99.9 wt%) of Mg, Ca and Zn were melted under an argon atmosphere in an induction furnace with the nominal composition (in atomic percentage). The master alloy was then remelted by induction melting in a quartz tube and injected into the copper mold with the diameter of 2 mm. The amorphous nature of the as-cast Mg–Zn–Ca samples was verified by X-ray diffraction (XRD) using a Rigaku DMAX 2400 diffractometer with CuK_α radiation and differential scanning calorimetry (DSC) (Perkin–Elmer, DSC-diamond) examination at a constant heating rate of 40 K/min. The as-cast Mg66Zn30Ca4 and Mg70Zn25Ca5 samples were further cut into 2 mm thick disks for the electrochemical tests with the surface being polished up to 2000 grit. All the samples were then ultrasonically cleaned in acetone, absolute ethanol and distilled water. For the cytocompatibility tests, the 2 mm thick disk samples were sterilized by ultraviolet-radiation for at least 2 h.

2.2. Mechanical tests

Uniaxial compression testing was conducted with an Instron 8562 testing machine at a constant nominal strain rate of $2 \times 10^{-4}\ s^{-1}$ at room temperature. The test samples with 2 mm in diameter and 4 mm in length were prepared according to ASTM standards.

2.3. Electrochemical tests

A three-electrode cell was used for electrochemical measurements. The counter electrode a platinum and the reference electrode a saturated calomel electrode (SCE). A wire lead was attached to the one round section of each sample and was closely sealed with epoxy resin leaving an-end surface (with a cross-section area of about 3.14 mm^2) exposed to solution. The electrochemical tests were conducted with an electrochemical workstation (CHI600C, China) at the temperature of 37 °C in simulated body fluid (SBF, NaCl 8.035 g, $NaHCO_3$ 0.355 g, KCl 0.225 g, $K_2HPO_4{\cdot}3H_2O$ 0.231 g, $MgCl_2{\cdot}6H_2O$ 0.311 g, $CaCl_2$ 0.292 g, Na_2SO_4 0.072 g, $(HOCH_2)_3CNH_2$ 6.118 g). The open circuit potentials (OCP) were monitored for 4000 s. The potentiodynamic polarization tests were carried out at a scanning rate of 1 mV/s and the initial potential was about 300 mV below the corrosion potential (E_{corr}) after 4000 s OCP measurements. After polarization testing, samples were washed with acetone, distilled water and finally air-dried. Changes in the surface morphologies were characterized by environmental scanning electron microscopy (ESEM, Quanta 200FEG). Afterwards, samples were immersed in chromic acid (180 g/l CrO_3) for 5–10 min to remove the corrosion products. The samples were then washed and dried again and were observed under ESEM. The XPS data were taken on an AXIS-Ultra instrument from Kratos Analytical using monochromatic AlK_α radiation (225 W, 15 mA, 15 kV) and low-energy electron flooding for charge compensation. To compensate for surface charge effect, binding energies were calibrated using C 1s hydrocarbon peak at 284.80 eV. The data were converted into VAMAS file format and imported into CasaXPS software package for manipulation and curve-fitting.

2.4. Indirect cytotoxicity evalution

Murine fibroblast cells (L929) and human osteosarcoma cells (MG63) were used in the vitro cell culture experiment. They were cultured in Dulbecco's modified Eagle's medium (DMEM), 10% fetal bovine serum (FBS), 100 U ml^{-1} penicillin and 100 μg ml^{-1} streptomycin at 37 °C in a humidified atmosphere of 5% CO_2.

The extraction media were prepared using DMEM serum free medium with the surface area/extraction medium ratio 1 cm^2/ml in a humidified atmosphere with 5% CO_2 at 37 °C for 72 h. The supernatant fluid was withdrawn and centrifuged to prepare the extraction medium, then refrigerated at 4 °C before the cytotoxicity test. The control groups involved the use of DMEM medium as negative control and 10% DMSO DMEM medium as positive control. Cells were incubated in 96-well cell culture plates at 5×10^3 cells/100 μl medium in each well and incubated for 24 h to allow attachment. The medium was then replaced with 100 μl of extraction medium. After incubating the cells in a humidified atmosphere with 5% CO_2 at 37 °C for 1, 3 and 5 days, respectively, the 96-well cell culture plates were observed under an optical microscope. After that, 10 μl MTT was added to each well. The samples were incubated with MTT for 4 h at 37 °C, and then 100 μl formazan solubilization solution (10%SDS in 0.01 M HCl) was added in each well overnight in the incubator in a humidified atmosphere. The spectrophotometrical absorbance of the samples was measured by microplate reader (Bio-RAD680) at 570 nm with a reference wavelength of 630 nm. The pH values and the concentrations of Mg, Zn and Ca ions in the extraction medium at different time point were also measured.

2.5. Direct cell adhesion experiment

200 μl cell suspension were seeded onto the Mg66Zn30Ca4 and Mg70Zn25Ca5 samples as well as the as-rolled pure magnesium sample (control) at a cell density of 1×10^5 (for L929 cell), 5×10^4 (for MG63 cells) cell/ml. After 1, 3 and 5 days culture in a humidified atmosphere with 5% CO_2 at 37 °C in 96-well plates, the parallel samples were fixed in 2.5% glutaraldehyde solution for 2 h at room temperature and rinsed 3 times with phosphate buffer solution (PBS, pH = 7.4), followed by dehydration in a gradient ethanol/distilled water mixture (50%, 60%, 70%, 80%, 90%, 100%) for 10 min each and dried in hexamethyldisilazane (HMDS) solution. The surface of cell adhered experimental samples was observed by ESEM. The pH values and the concentrations of magnesium and alloying element ions in the culture medium were also measured for each culture interval.

3. Results

3.1. Microstructure and mechanical properties

Fig. 1 shows the XRD patterns of as-rolled pure Mg, Mg66Zn30Ca4 and Mg70Zn25Ca5. The typical amorphous features of two Mg–Zn–Ca samples can be confirmed by the absence of detectable crystalline diffraction peaks, together with the broad scattering signals around 38° and 66°. The broad scattering maximum peak of Mg70Zn25Ca5 sample shifts slightly toward the low angle side, compared with Mg66Zn30Ca4 sample, which can be attributed to its slightly higher Mg content since we know that Mg has a larger atomic radius than Zn does [15].

Fig. 2 shows the corresponding DSC curves of Mg66Zn30Ca4 and Mg70Zn25Ca5. The glass transition temperature (T_g) and the first crystallization temperature (T_{x1}) of Mg66Zn30Ca4 sample are higher than those of Mg70Zn25Ca5 sample. Zhao et al. [19] also observed that with the increase of the Mg content in the Mg–Zn–Ca glasses both the T_g and T_{x1} decreased.

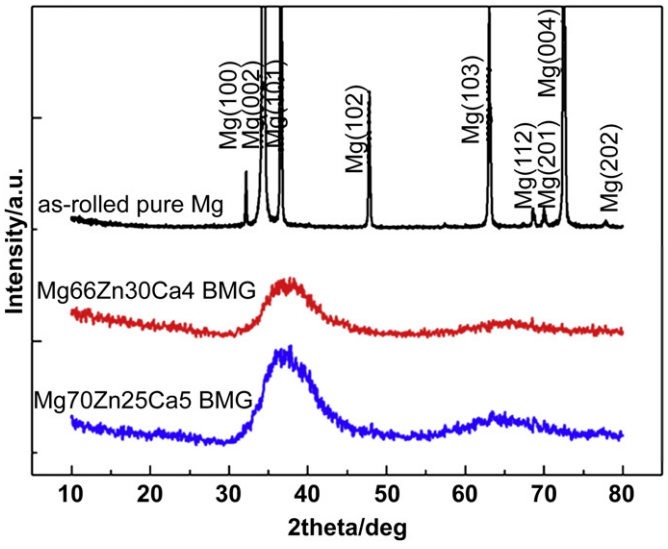

Fig. 1. XRD patterns of as-rolled pure Mg, Mg66Zn30Ca4 and Mg70Zn25Ca5.

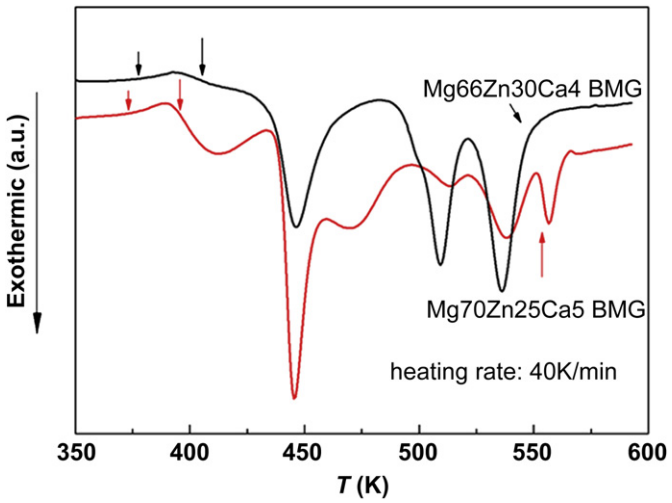

Fig. 2. DSC measurement of Mg66Zn30Ca4 and Mg70Zn25Ca5.

Fig. 3 presents the typical compression stress–strain curves of Mg66Zn30Ca4 and Mg70Zn25Ca5 samples. The fracture strength σ_f for Mg70Zn25Ca5 and Mg66Zn30Ca4 samples is (565.8 ± 23.2) and (531.2 ± 22.8) MPa, respectively, which is much higher than that of pure Mg sample (198.1 ± 4.5) MPa [20].

3.2. Electrochemical measurements

Fig. 4 shows the OCP curves and potentiodynamic polarization curves of as-rolled pure Mg, Mg66Zn30Ca4 and Mg70Zn25Ca5 at 37 °C in SBF. The OCP values of the two Mg–Zn–Ca samples shift toward the positive potential fast in the initial 1000 s, and clearly they are higher than that of as-rolled pure Mg sample. Mg66Zn30Ca4 sample indicates a more positive OCP value than that of Mg70Zn25Ca5 sample, possibly attributed to the different amount of Zn in the two Mg–Zn–Ca samples, since the electrode potential of Zn ($-1.02V_{SCE}$) is more positive than Mg ($-1.65V_{SCE}$) [9]. In addition, obvious fluctuation can be observed for the OCP curves of Mg70Zn25Ca5 and as-rolled pure Mg samples, whereas Mg66Zn30Ca4 sample exhibits more steady OCP value. As shown in Fig. 4(b), the two Mg–Zn–Ca samples show reduced kinetics of anodic and cathodic reactions than that of as-rolled pure Mg sample. Alloying with the more noble component Zn can give rise to a strong diminution of the well-known reaction of Mg with water under hydrogen evolution [21,22]. The I_{corr} of Mg66Zn30Ca4, Mg70Zn25Ca5 and as-rolled pure Mg samples are 3.53 μA/cm^2, 11.2 μA/cm^2 and 36.8 μA/cm^2, respectively. It can be inferred from the above results that the two Mg–Zn–Ca samples show improved corrosion resistance comparing with the as-rolled pure Mg sample, with Mg66Zn30Ca4 better than Mg70Zn25Ca5.

Fig. 5 shows the SEM images of experimental samples after polarization. The surface of Mg66Zn30Ca4 after polarization is relatively homogeneous and even with few cracks, whereas a rough surface with obvious deep cracks can be seen with Mg70Zn25Ca5 and as-rolled pure Mg. After removing the corrosion products, many micro-pores can be seen for Mg66Zn30Ca4 (2–10 μm), compared with the relatively large and uneven distributed holes beneath the surface of as-rolled pure Mg (10–60 μm). The XPS results indicate that the compositions of the corrosion product film of the Mg–Zn–Ca samples are Mg, Zn, Ca, P and O. The ZnO and O^{2-} species are much richer at the surface of Mg66Zn30Ca4 than that of Mg70Zn25Ca5.

3.3. Immersion tests

Fig. 6 shows the change of pH values for the SBF incubating as-rolled pure Mg and Mg–Zn–Ca samples. The Mg66Zn30Ca4

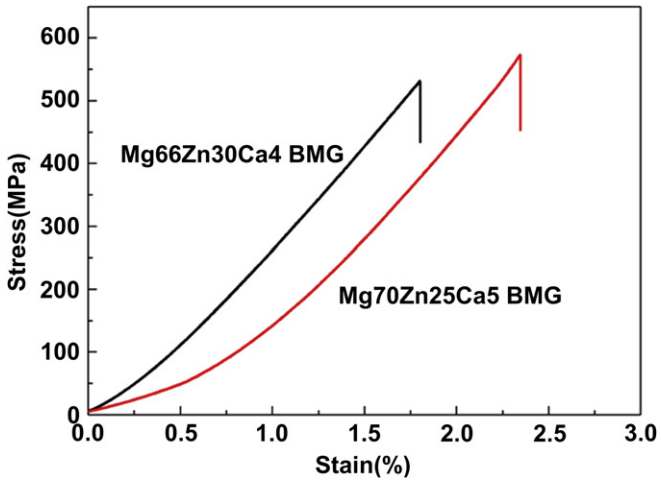

Fig. 3. Compression properties of Mg66Zn30Ca4 and Mg70Zn25Ca5.

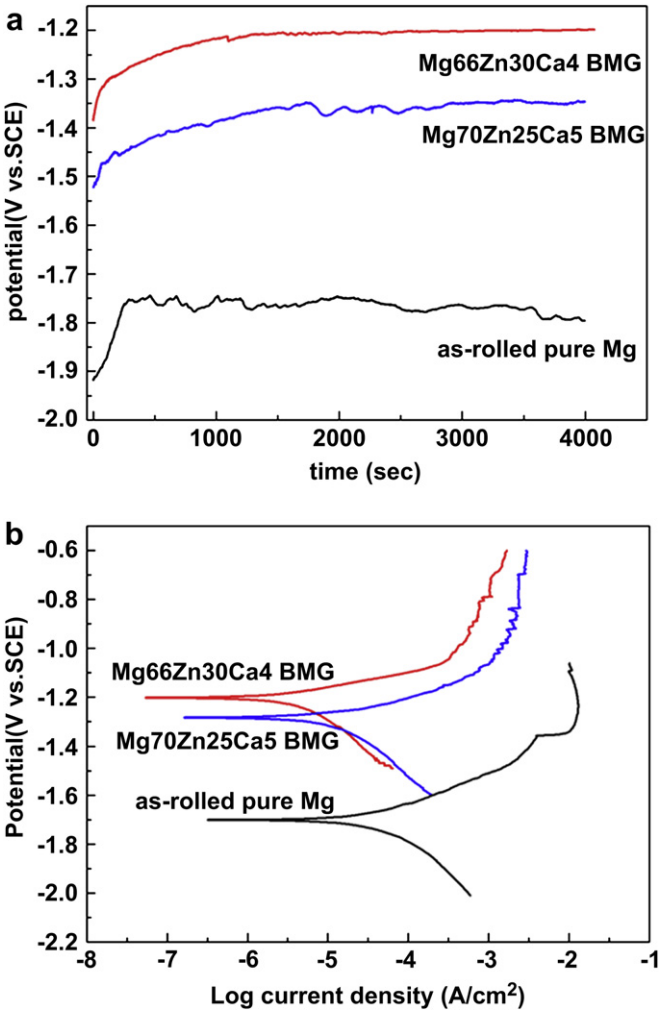

Fig. 4. (a) OCP curves and (b) potentiodynamic polarization curves of as-rolled pure Mg, Mg66Zn30Ca4 and Mg70Zn25Ca5.

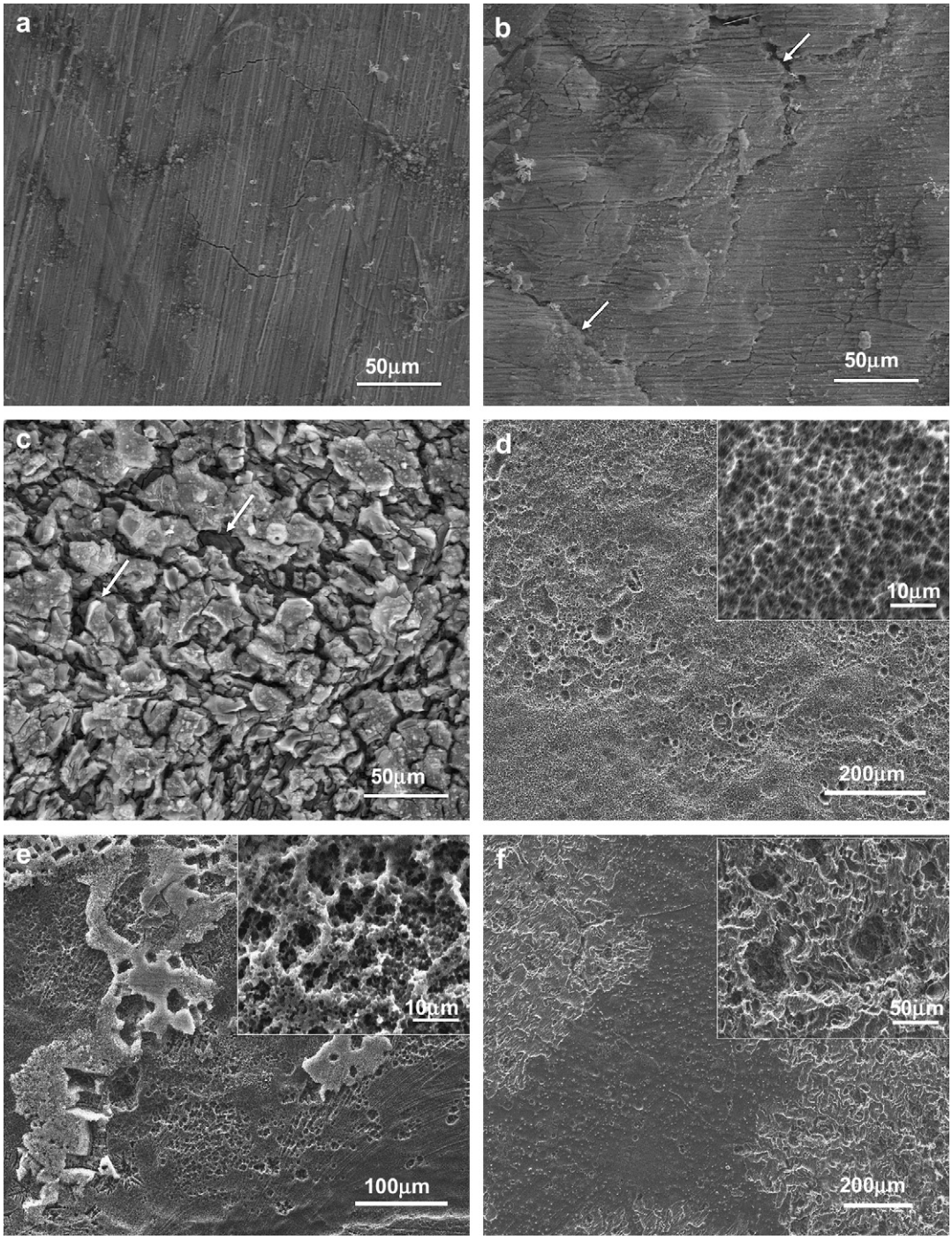

Fig. 5. SEM images showing the surface morphologies of (a) Mg66Zn30Ca4, (b) Mg70Zn25Ca5 and (c) as-rolled pure Mg after polarizations in SBF at 37 °C; SEM images showing the surface morphologies of (d) Mg66Zn30Ca4, (e) Mg70Zn25Ca5 and (f) as-rolled pure Mg after immersing in CrO_3 solution for 10 min.

exhibited a slower change of pH than that of as-rolled pure Mg and Mg70Zn30Ca5. Moreover, the as-rolled pure Mg and Mg70Zn25Ca4 disintegrated into several parts and further observation was not carried out.

Fig. 7 shows the surface morphologies of as-rolled pure Mg, Mg66Zn30Ca4 and Mg70Zn25Ca5 samples immersed in SBF for different times. The Mg66Zn30Ca4 shows a flat surface, after 3 d immersion in SBF at 37 °C, with the surface composition including C, O, Mg, P, Ca, Zn and the Zn content is extremely high compared to Mg content. In the case of Mg70Zn25Ca5, some micro-pores are visible on the surface and the EDS results indicate that the Zn content is higher than Mg content, whereas the difference value is not as large as that for Mg66Zn30Ca4 sample. After 30 d immersion, Mg66Zn30Ca4 sample almost maintains the original geometric configuration. The observations show that a compact and uniform corrosion product layer forms on the surface of Mg66Zn30Ca4 sample and the Mg content in the corrosion product layer is slightly higher than the Zn content. Moreover, the O content increases greatly with the prolonged immersion time. In contrast, as-rolled pure Mg shows a crackled surface after 3 d immersion and the surface compositions are O, Mg, P and Ca.

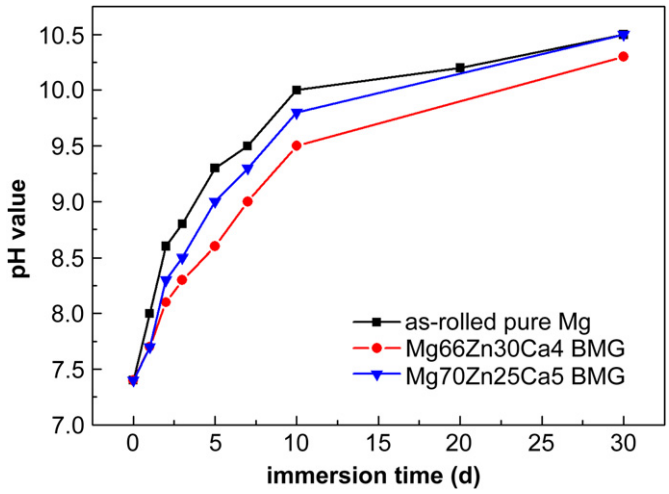

Fig. 6. The change of pH values of the SBF incubating as-rolled pure Mg, Mg66Zn30Ca4 and Mg70Zn25Ca5 during 30 d immersion.

3.4. Cytotoxicity measurements

Fig. 8 shows the cytotoxicity results of Mg66Zn30Ca4 and Mg70Zn25Ca5 samples for indirect and direct cell assay using L929 and MG63 cells. It can be concluded that Mg66Zn30Ca4 and Mg70Zn25Ca5 extracts indicate improved cell viability for the two cell lines, compared with as-rolled pure Mg extract. The cell viability obtained in indirect assay is higher than that obtained in direct assay. Furthermore, Mg66Zn30Ca4 sample shows higher cell viability than that of Mg70Zn25Ca5 sample.

Fig. 9 shows the morphologies of L929 and MG63 cells cultured on as-rolled pure Mg, Mg66Zn30Ca4 and Mg70Zn25Ca5 samples for 5 days. For the as-rolled pure Mg sample, a few cells are observed on the surface after 1 day culture. After 3 days culture, much elongated cell morphology and increased cell number can be seen, whereas unhealthy cells with round shape can be seen after 5 days culture for the two experimental cell lines. For Mg66Zn30Ca4, the number of cells adhered on the surface is also few on day 1, whereas increased cell number with healthy cell morphologies is observed after 3 and 5 days culture. In the case of Mg70Zn25Ca5, few cells adhere on its surface on day 1. Thereafter, the cells number increases slowly on day 3 and day 5, compared with that for Mg66Zn30Ca4. It is noted that the micro-cracks can be seen on the Mg70Zn25Ca5 after 5 days culture (Fig. 9(c)) and sometime samples disintegrate into several parts.

Fig. 10 shows the release of Mg, Zn and Ca into the extraction medium at days 1, 3 and 5. Mg66Zn30Ca4 extraction medium and DMEM culturing with Mg66Zn30Ca4 show lowest Mg ions concentrations, compared with that of the Mg70Zn25Ca5 and as-rolled pure Mg samples. The Mg ions in the culture medium of Mg70Zn25Ca5 indicate a close amount compared with that for as-rolled pure Mg. In addition, the culture medium for

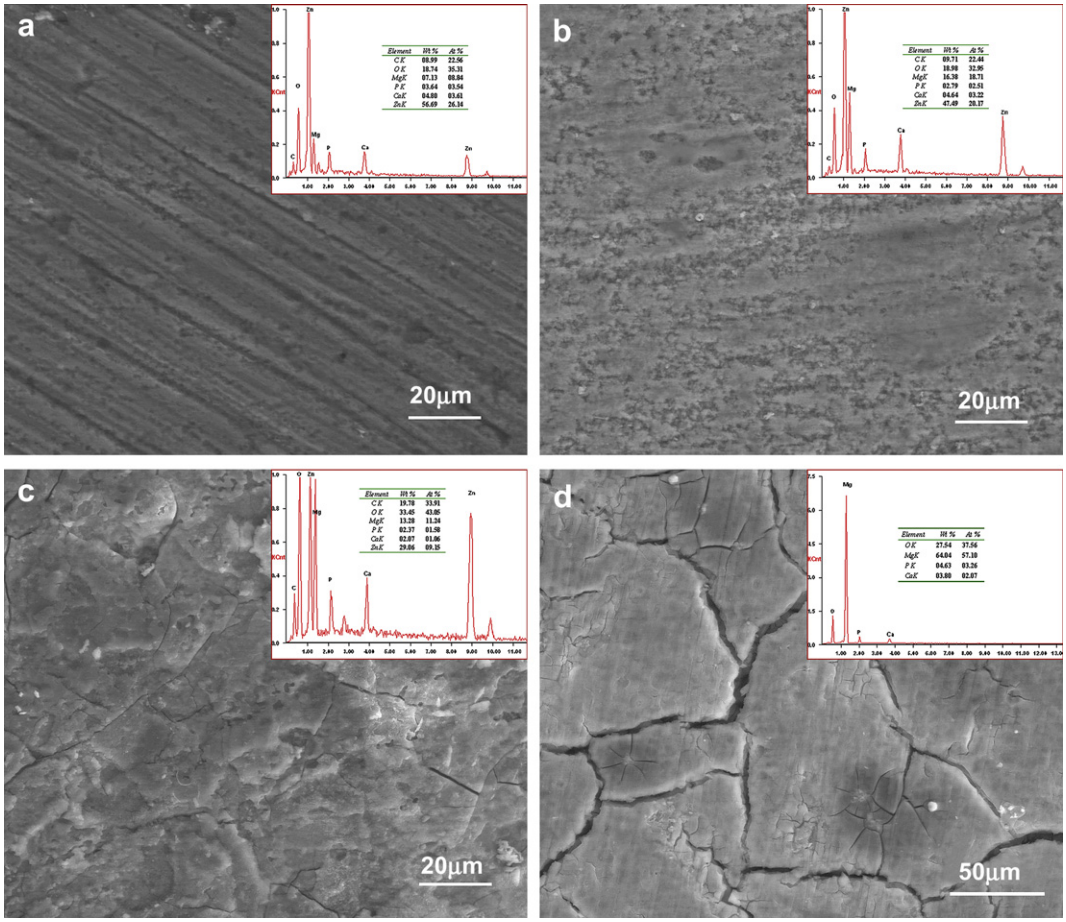

Fig. 7. The surface morphologies and compositions of (a) Mg66Zn30Ca4, (b)Mg70Zn25Ca5 and (d) as-rolled pure Mg after 3 d immersion in SBF at 37 °C; and the surface morphologies and compositions of (c) Mg66Zn30Ca4 after 30 d immersion in SBF at 37 °C.

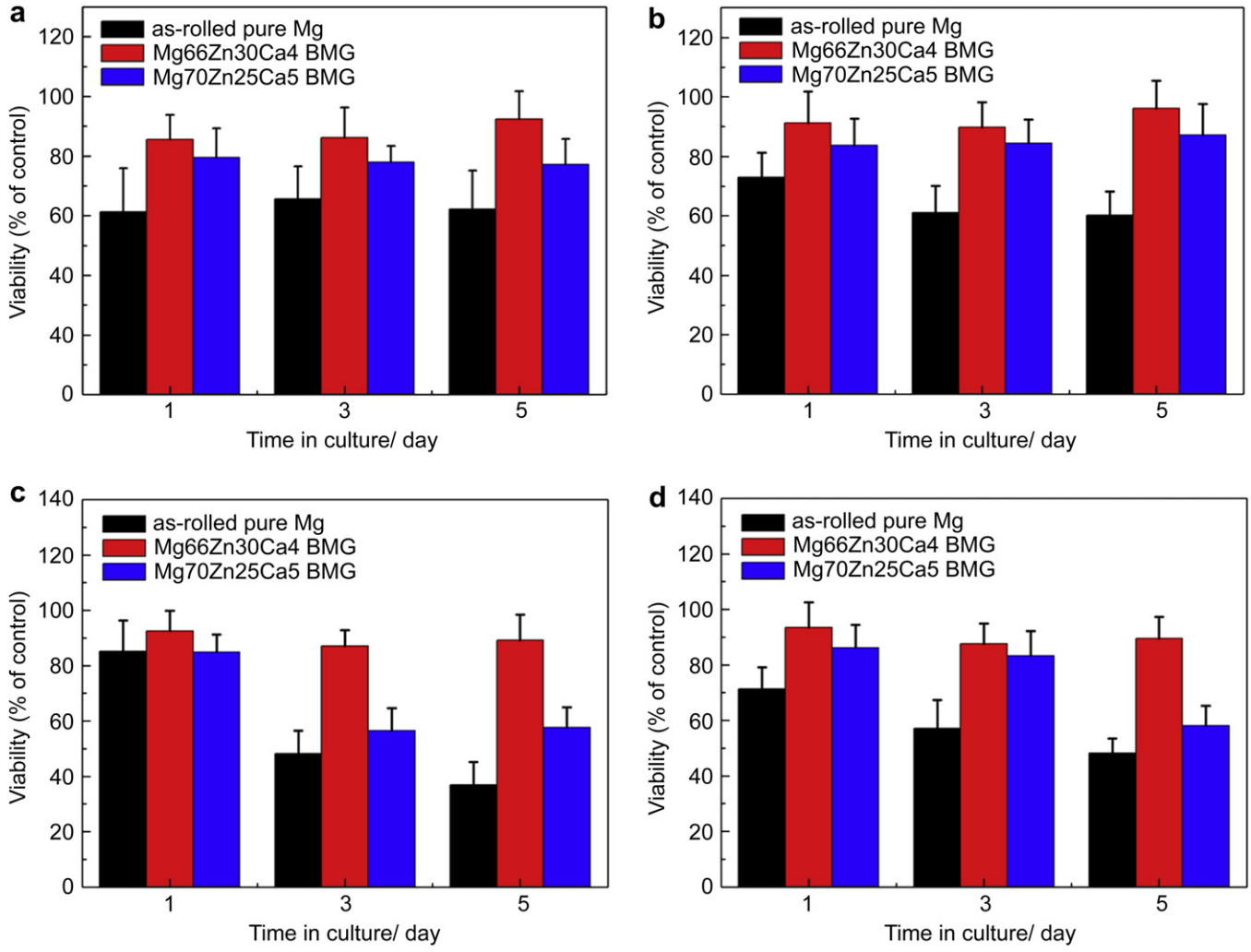

Fig. 8. Cytotoxicity of (a) L929 and (b) MG63 cells cultured in as-rolled pure Mg, Mg66Zn30Ca4 and Mg70Zn25Ca5 extraction mediums; and the cytotoxicity of (c) L929 and (d) MG63 cells cultured with as-rolled pure Mg, Mg66Zn30Ca4 and Mg70Zn25Ca5 samples directly.

Mg70Zn25Ca5 shows almost equal amount of Ca ions but much higher amount of Zn ions, compared with that from Mg66Zn30Ca4.

The pH values of as-rolled pure Mg, Mg66Zn30Ca4 and Mg70Zn25Ca5 extractions medium and DMEM culturing with L929 and MG63 cells for 1, 3 and 5 days are shown in Fig. 11. It can be seen that, during the 5 days incubation period, the pH value of DMEM culturing with the as-rolled pure Mg and two Mg–Zn–Ca samples slightly increase with the prolonged incubation time. The medium culturing with as-rolled pure Mg shows higher pH value than that of Mg70Zn25Ca5, and the medium incubating Mg66Zn30Ca4 sample indicates the lowest pH value. There is no obvious change in pH values between the L929 and MG63 cells group. Moreover, the extract mediums, incubating the experimental samples without serum and cells for 3 days, show slightly higher pH values than the DMEM incubating the experimental samples with serum and cells.

4. Discussion

Recent studies on magnesium-based alloys as biodegradable materials have demonstrated that high mechanical properties and minimized corrosion rate are required for clinical applications. The Mg–Zn–Ca materials are clearly of good potential.

4.1. Comparison of the mechanical properties of Mg–Zn–Ca glass with as-reported biomedical Mg alloys

Fig. 12(a) presents the mechanical properties comparison of the previously reported Mg alloys and cortical bone as well as that of present Mg66Zn30Ca4 and Mg70Zn25Ca5. The two Mg–Zn–Ca glasses show and may exhibit higher strength after partial deterioration process during the degradation period. The elastic modulus of the Mg–Zn–Ca samples is closer to those of cortical bone, compared with the other biomedical Mg alloys. The different mechanical properties of the Mg–Zn–Ca samples and the Mg alloys can be attributed to the differences in their intrinsic local structure. Samples are single-phase, chemically homogeneous, with the absence of the easy crystal slip systems than crystalline Mg alloys and therefore exhibit higher strength.

4.2. Comparison of the corrosion behavior of Mg–Zn–Ca glass with as-reported biomedical Mg alloys

As can be seen from Fig. 12(b), Mg66Zn30Ca4 and Mg70Zn25Ca5 samples show reduced corrosion rates, compared to other previously reported Mg alloys, as calculated according to ASTM-G102-89 [25]. On the one hand, it can be attributed to the chemical homogeneity and the absence of the second phase in Mg–Zn–Ca even added with

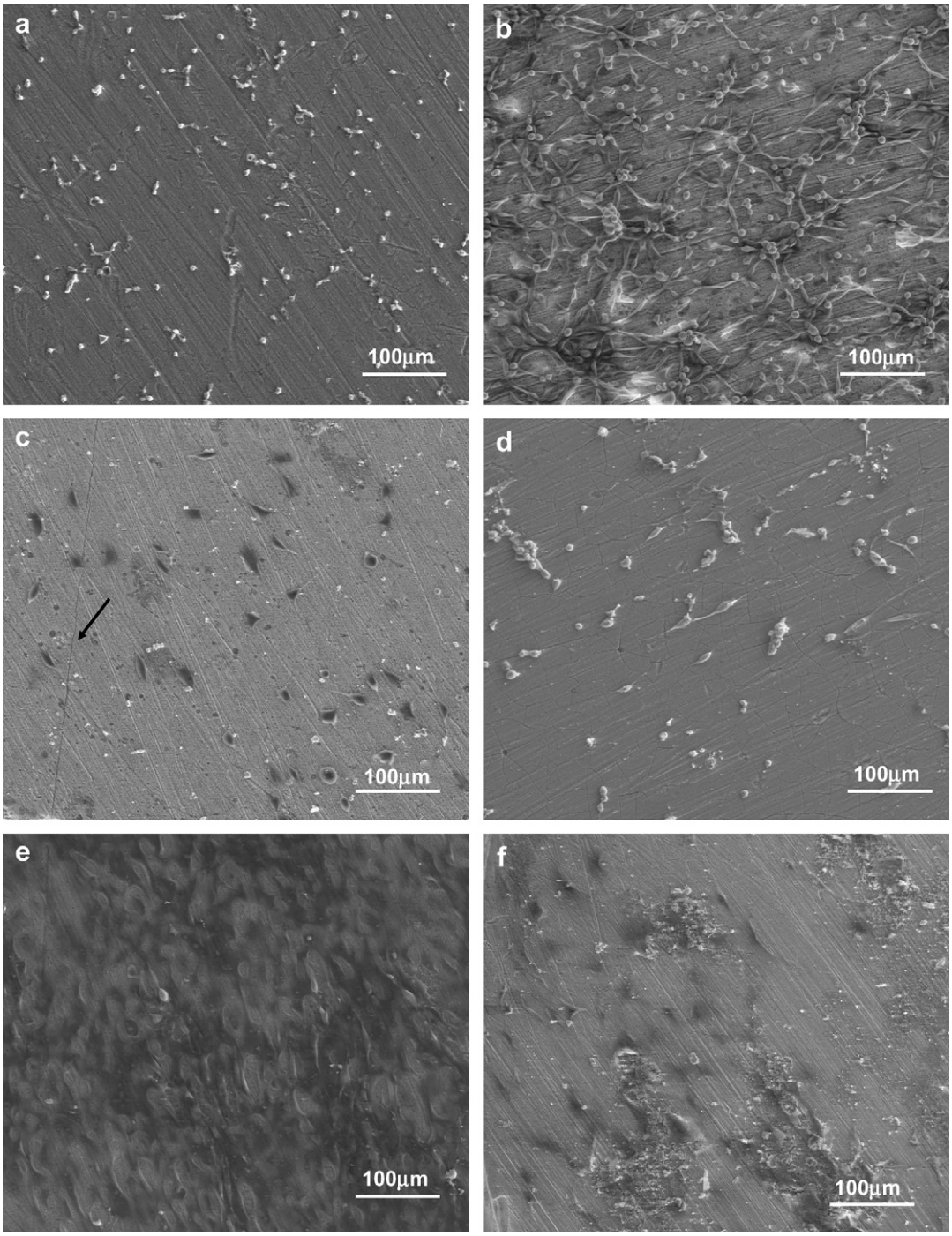

Fig. 9. The morphology of (a–c) L929 and (d–f) MG63 cells cultured on (a,d) as-rolled pure Mg, (b,e) Mg66Zn30Ca4 and (c,f) Mg70Zn25Ca5 samples for 5 days.

a high Zn content exceeding its solid solubility in Mg matrix. This homogeneous structure, which minimizes the galvanic corrosion, may be also the reason forming the more uniform corrosion surface morphologies for the Mg–Zn–Ca samples than that of the as-rolled pure Mg. On the other hand, the formation of zinc oxide/hydroxide together with magnesium oxide/hydroxide or formation of a double oxide/hydroxide to give a continuous and uniform coverage of the Mg–Zn–Ca samples surface also plays an important role. The EDS results show the presence of zinc (oxide/hydroxide), which is even higher than magnesium (oxide/hydroxide) in the initial 3 d immersion periods. Furthermore, the different corrosion behaviors between two Mg–Zn–Ca samples may be attributed to the higher content of Zn in Mg66Zn30Ca4. Similarly, Li [26] showed that Mg65Cu20Zn5Gd10 possessed better corrosion resistance than Mg65Cu25Gd10 which had been attributed to the existence of Zn in the former. In addition, the micro-alloying with Ca, about 0.04 wt% in Mg66Zn30Ca4 and 0.06 wt% in Mg70Zn25Ca5, may be also advantageous to the enhancement of corrosion resistance. It had been widely revealed that Ca had beneficial effect on the corrosion behaviors of magnesium alloys [4,27,28] with less than 1 wt% alloying but a deleterious effect while the adding Ca content exceeding 1 wt% [5,28,29].

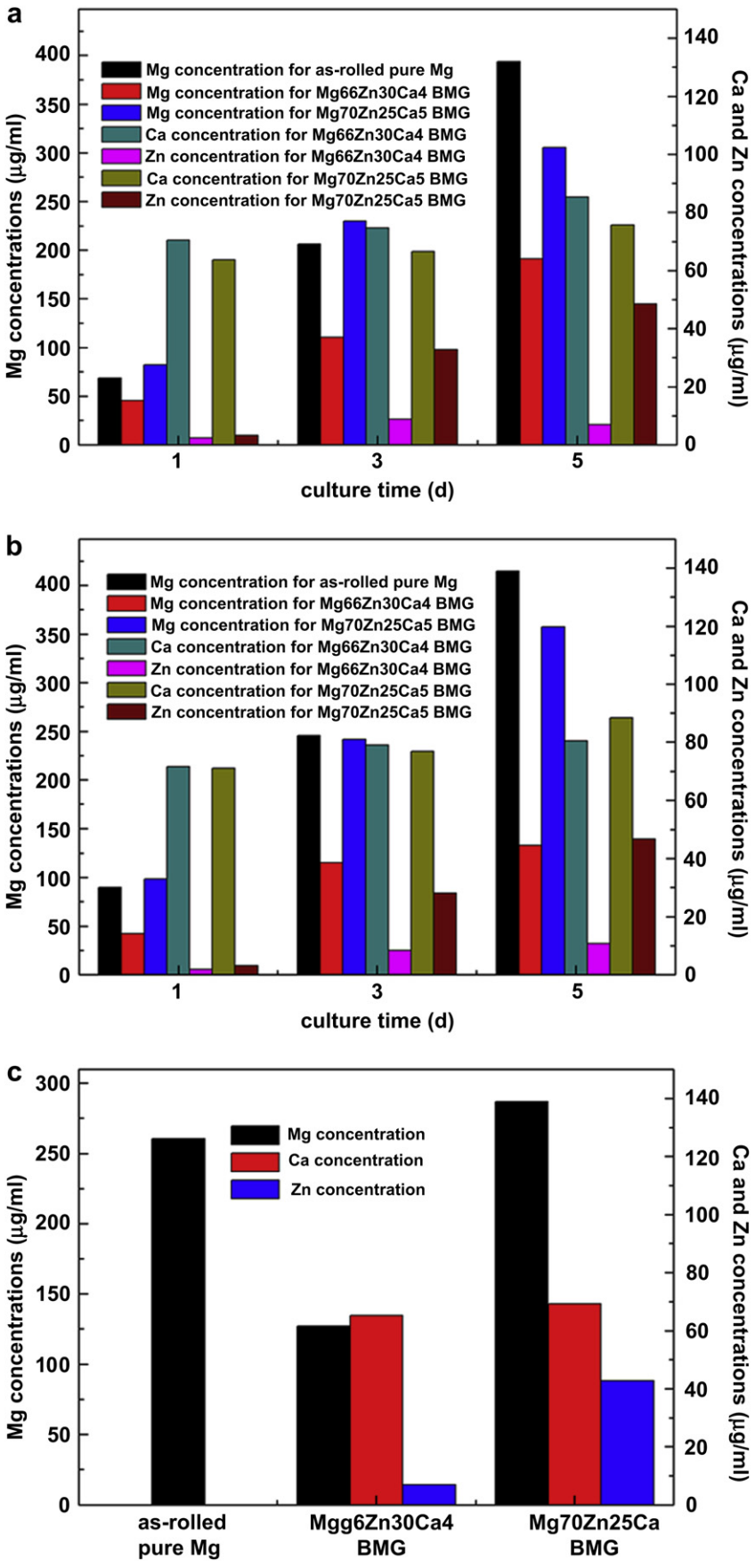

Fig. 10. The element releasing of Mg, Ca and Zn in culture medium DMEM with (a) L929 and (b) MG63 cells for 1, 3 and 5 days and (c) extraction medium.

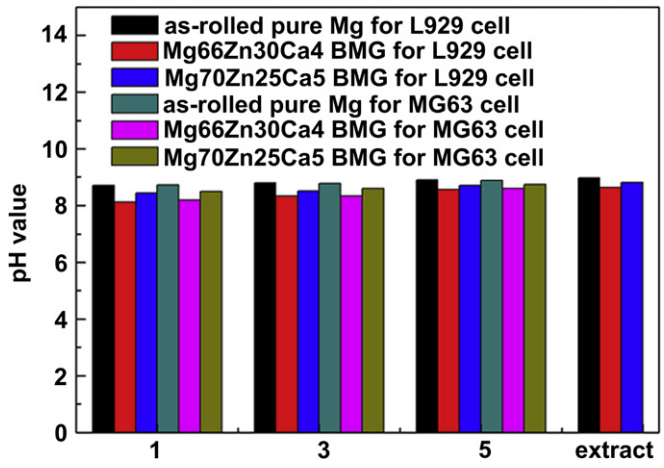

Fig. 11. The pH values of culture medium DMEM with L929 and MG63 for 1, 3 and 5 days and extraction medium incubating as-rolled pure Mg, Mg66Zn30Ca4 and Mg70Zn25Ca5 samples.

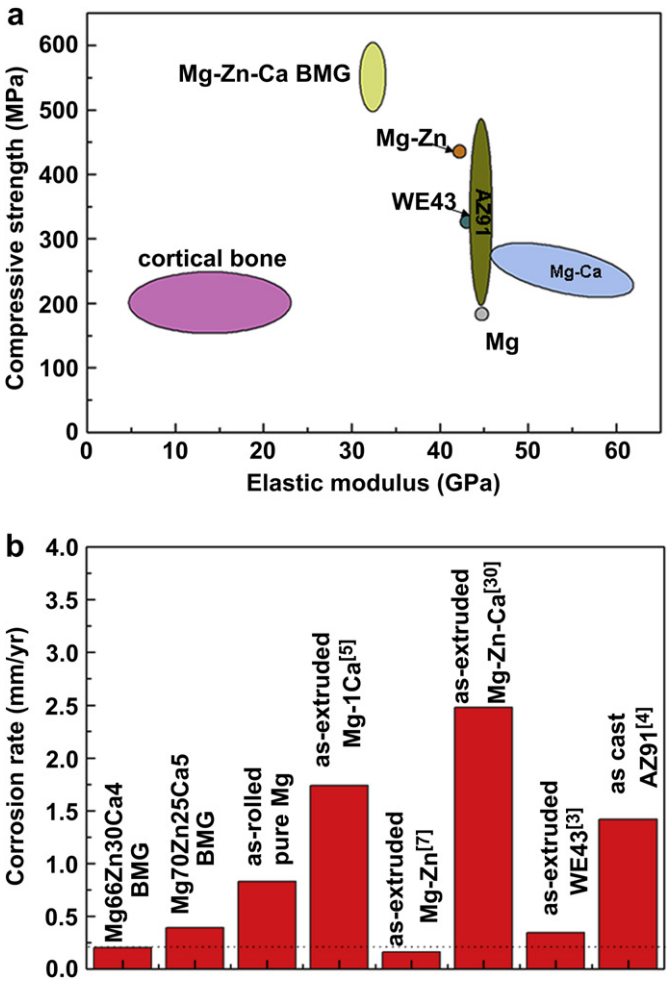

Fig. 12. The comparison of (a) the mechanical properties and (b) corrosion behavior among Mg66Zn30Ca4 and Mg70Zn25Ca bulk metallic glasses as well as the as-reported biomedical Mg alloys [5,7,16,23,24].

The evolution of the corrosion process of the Mg–Zn–Ca glass is schematically illustrated in Fig. 13 based on the morphologies and compositions of surface corrosion product layer in the present study. (1) When the Mg–Zn–Ca sample is immersed in body fluid, the anodic dissolution of magnesium occurs and the magnesium hydroxide layer will be formed on the surface of the sample. The attack of Cl^- occurs at the weak sites of the magnesium hydroxide layer and transforms the magnesium hydroxide into soluble magnesium chloride. The fresh substrate, exposed to the medium directly, suffers further corrosion and results in the releasing of Mg^{2+} and Zn^{2+} (Fig. 13(a)). (2) When the immersion time is prolonged, the Zn^{2+} concentration is promoted due to the continuous dissolution of Zn. Thereafter, $Zn(OH)_2$ precipitates preferentially, with the low solubility K_{sp} (1.8×10^{-14} [30]), compared to that of $Mg(OH)_2$ (5.61×10^{-12} [30]), which will also result in a better protection effect than the case of single $Mg(OH)_2$ precipitates. As shown in Fig. 13(b), the $Zn(OH)_2$ precipitations will repair the defects in the surface layer because the higher content of OH^- with the dissolution of $Mg(OH)_2$, and then form a continuous and uniform layer on the surface of the Mg–Zn–Ca sample. (3) With the corrosion proceeds, the corrosion product layer will be thickened and the $Zn(OH)_2$ precipitates spread, which are evidently depicted in Fig. 13(c). Meanwhile, the undissolved $Mg(OH)_2$ and $Zn(OH)_2$ precipitation area on the surface of the Mg–Zn–Ca sample is considered to provide favorable sites for apatite nucleation [31]. Consequently, lots of apatite nuclei are formed on the corrosion product layer and then apatite will grow spontaneously by consuming the calcium and phosphate from the surrounding medium [31].

4.3. Comparison of the in vitro biocompatibility of Mg–Zn–Ca glass with as-reported biomedical Mg alloys

The results of the indirect cytotoxicity tests show that the present Mg–Zn–Ca samples exhibit similar cytotoxicity Grades 0–1 (according to ISO 10993-5:1999 [32]) as the investigated Mg–Ca [5], Mg–Zn [7] and Mg–Zn–Ca alloys [23], which proves their biosafety for further biomedical applications. In the case of the direct assay, the present study indicates well adhered cells on the surface of the Mg66Zn30Ca4 sample as well as 0–1 cytotoxicity Grades. The good adhesion of the osteoblast-like and elliptical cells was also observed on the surface of Mg–0.51 wt%Ca alloy whereas statistically significant decreases ALP activity and total protein were seen after 8 day cell culture [29]. Zhang et al. [33] reported the early adhesion of MC3T3-E1 cells on the surface of Mg–Zn alloys and pointed out that the peeling off of some corrosion layer will weaken the adhesion of cell. This phenomenon is also seen in the case of as-rolled pure Mg from the corroded surfaces observation with some deep pits on the surfaces. However, few peeling off of the corrosion layer can be seen for the Mg66Zn30Ca4 with combined protection by magnesium hydroxide and zinc hydroxide. Xu et al. [34] found that only a few L929 cells were observed on the naked Mg–Mn–Zn alloy surface after 1-day culture and the number of the cells increased slowly after 3-day and 5-day culture periods (about 700/mm^2, deduced from Fig. 7 in [34]). In the present study, about a number of 1000/mm^2 cells adhered on the surface of the Mg66Zn30Ca4 samples after 3-day culture time, which was comparable to the Ca–P coated Mg–Mn–Zn alloy and pure Ti in reference [34].

As reported by Witte et al. [35], the direct cell assay leads to the reduced cell viability than the indirect cytotoxicity tests. It is known that cells are very sensitive to the environment fluctuation (including ion releasing, pH changes, hydrogen evolution, the disintegrated particles and corrosion product $Mg(OH)_2$ for Mg-based biomaterials) and the influencing factors would increase when the cells culture with the experimental material directly. Firstly, the reduced cell viability in the direct assay may be attributed to the hydrogen evolution, since no distinct differences can be seen from

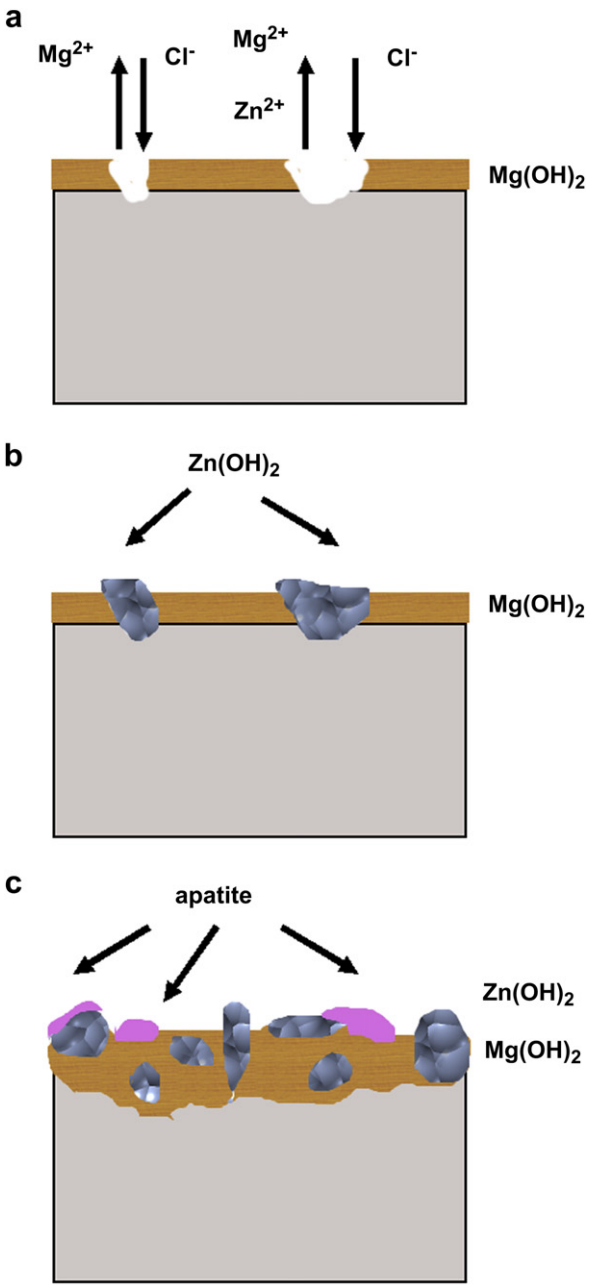

Fig. 13. The sketch map for the evolution of corrosion process of Mg–Zn–Ca bulk metallic glass immersed in SBF. (a) Initial stage; (b)Middle stage; (c) Final stage.

the ion releasing and pH changes results from the indirect and direct assays (Figs. 10 and 11). And the L929 cells did not show toxicity (RGR at 0 cytotoxicity Grades) while the Mg and Zn concentration is up to 1000 mg/L and 60 mg/L [36], which was much higher than the concentration obtained in this study. Once a Mg-based material is immersed in the cell culture medium, the hydrogen gas will evolve from the surface of the sample which may deteriorate the cells adhesion and the following proliferation process. Secondly, with the high pH value, magnesium hydroxide and zinc hydroxide will precipitate easily during the incubation period not only on the surface of sample but also in the culture medium. Witte et al. [37] reported the presence of small corrosion products at the micro-scale size inside the giant cells. It was assumed that micro-size $Mg(OH)_2$ might not be extremely toxic to cells in the consideration of slight toxicity can be seen for nano-scale MgO particles [38]. However, the toxicity of micro-size $Zn(OH)_2$ may be related to the concentration of the particles. Lin et al. [39] reported the micro-sized ZnO particles (420 nm) did not induce statistically significant toxicity ($p < 0.05$) to the human bronchoalveolar carcinoma-derived cell line (A549) at the dosage lower than 10 μg/ml. Nair et al. [40] indicated that micro-ZnO is extremely toxic (about 50% reduced cell viability) to MG63 cell at concentration above 100 μM. Thirdly, the forming cracks and the disintegration of Mg70Zn25Ca5 sample may also contribute to the poor adhesion and cell viability compared to Mg66Zn30Ca4 sample.

5. Conclusions

In this study, Mg66Zn30Ca4 and Mg70Zn25Ca5 bulk metallic glass were prepared. They showed close compression strength, three times of the compression strength of pure Mg. They also exhibited improved corrosion potential and reduced current densities compared to as-rolled pure Mg. Their surfaces show much more even corrosion morphologies, with more uniformly distributed micro-pores than those with a larger and quite different scale pores enveloping on the surface of as-rolled pure Mg. The corrosion product layer, formed on the two Mg–Zn–Ca samples after 3 d immersion, exhibits higher Zn content than Mg, and thereafter a comparable content of Zn and Mg and increased O content can be seen after 30 d. The indirect and direct cytocompatibility tests show that Mg66Zn30Ca4 and Mg70Zn25Ca5 samples indicate higher cell viability than that of as-rolled pure Mg. Moreover, L929 and MG63 cells are found to be well adhered and proliferated on the surface of the Mg66Zn30Ca4 samples.

Acknowledgements

This work was supported by the National Natural Science Foundation of China (No. 30670560 and 30770580) and Program for New Century Excellent Talents in University (NCET-07-0033).

Appendix

Figures with essential color discrimination. Figs. 1–4, 6–8, 10–13 in this article are difficult to interpret in black and white. The full color images can be found in the on-line version, at doi:10.1016/j.biomaterials.2009.11.015

References

[1] Witte F, Kaese V, Switzer H, Meyer-Lindenberg A, Wirth CJ, Windhag H. In vivo corrosion of four magnesium alloys and the associated bone response. Biomaterials 2005;26:3557–63.
[2] Witte F, Fischer J, Nellesen J, Crostack H, Kaese V, Pischd A, et al. In vitro and in vivo corrosion measurements of magnesium alloys. Biomaterials 2006;27:1013–8.
[3] Xu L, Yu G, Zhang E, Pan F, Yang K. In vivo corrosion behavior of Mg–Mn–Zn alloy for bone implant application. J Biomed Mater Res 2007;83A(3):703–11.
[4] Kannan MB, Raman RKS. In vitro degradation and mechanical integrity of calcium-containing magnesium alloys in modified-simulated body fluid. Biomaterials 2008;29:2306–14.
[5] Li Z, Gu X, Lou S, Zheng Y. The development of binary Mg–Ca alloys for use as biodegradable materials within bone. Biomaterials 2008;29:1329–44.
[6] Staiger MP, Pietaka AM, Huadmaia J, Dias G. Magnesium and its alloys as orthopedic biomaterials: a review. Biomaterials 2006;27:1728–34.
[7] Zhang S, Zhang X, Zhao C, Li J, Song Y, Xie C, et al. Research on an Mg–Zn alloy as a degradable biomaterial. Acta Biomater 2009;. doi:10.1016/j.actbio.2009.06.028.
[8] Song G, Atrens A. Corrosion mechanisms of magnesium alloys. Adv Eng Mater 1999;1(1):11–33.
[9] Song G, Atrens A. Understanding magnesium corrosion-a framework for improved alloy performance. Adv Eng Mater 2003;5(12):837–58.
[10] Song GL. Control of biodegradation of biocompatible magnesium alloys. Corros Sci 2007;49:1696–701.

[11] Gu X, Zheng Y, Cheng Y, Zhong S, Xi T. In vitro corrosion and biocompatibility of binary magnesium alloys. Biomaterials 2009;30:484–98.
[12] Wang WH, Dong C, Shek CH. Bulk metallic glasses. Mater Sci Eng R Rep 2004;44(2–3):45–89.
[13] Scully JR, Gebert A, Payer JH. Corrosion and related mechanical properties of bulk metallic glasses. J Mater Res 2007;22:302–13.
[14] Gebert A, Wolff U, John A, Eckert J, Schultz L. Stability of the bulk glass-forming $Mg_{65}Y_{10}Cu_{25}$ alloy in aqueous electrolytes. Mater Sci Eng A Struct Mater 2001;299:125–35.
[15] Gu X, Shiflet GJ, Guo FQ, Poon SJ. Mg–Ca–Zn bulk metallic glasses with high strength and significant ductility. J Mater Res 2005;20(8):1935–8.
[16] www.magnesium-elektron.com.
[17] Sigel Helmut. Metal ions in biological system. In: Concepts on metal ion toxicity, vol. 20. Marcel Dekker, Inc.; 1986.
[18] Seiler Hans G, Sigel Helmut, Sigel Astrid. Handbook on toxicity of inorganic compounds. Marcel Dekker, Inc.; 1988.
[19] Zhao YY, Ma E, Xu J. Reliability of compressive fracture strength of Mg–Zn–Ca bulk metallic glasses: flaw sensitivity and Weibull statistics. Scr Mater 2008;58:496–9.
[20] Wan Y, Xiong G, Luo H, He F, Huang Y, Zhou X. Preparation and characterization of a new biomedical magnesium–calcium alloy. Mater Des 2008;29(10):2034–7.
[21] Ghali E, Dietzel W, Kainer KU. General and localized corrosion of magnesium alloys: a critical review. J Mater Eng Perform 2004;13:7–23.
[22] Gebert A, Haehnel V, Park ES, Kim DH, Schultz L. Corrosion behavior of $Mg_{65}Cu_{7.5}Ni_{7.5}Ag_5Zn_5Gd_5Y_5$ bulk metallic glass in aqueous environments. Electrochim Acta 2008;53:3403–11.
[23] Guan S, Lei L, Wang L, Ren C, Zhu S, Wang H. In vitro degradation and mechanical integrity of Mg-Zn-Ca alloy coated with calcium-deficient hydroxyapatite by pulse electrodeposition process. THERMEC'; 2009. In: International conference on progressing & manufacturing of advanced materials, Biomaterials & Biomedical Applications I – 1st Symposium on degradable metals for biomedical applications.
[24] Witte F, Hort N, Vogt C, Cohen S, Kainer KU, Willumeit R, et al. Degradable biomaterials based on magnesium corrosion. Curr Opin Solid State Mater Sci 2008;12(5–6):63–72.
[25] ASTM-G102–89. Standard practice for calculation for corrosion rates and related information from electrochemical measurements. Annual book of ASTM standards. Philadephia, Pennsylvania. USA: American Society for Testing and Materials; 1999.
[26] Li G, Huang W, Li H, Zheng L, Hashmi MF. Corrosion behavior of $Mg_{65}Cu_{25-x}Zn_xGd_{10}$ ($x = 0,5$) metallic glass. J Wuhan Univ Technol Mater Sci 2008;23(5):678–82.
[27] Zhang E, Yang L. Microstructure, mechanical properties and bio-corrosion properties of Mg–Zn–Mn–Ca alloy for biomedical application. Mater Sci Eng A 2008;497:111–8.
[28] Kim W-C, Kim J-G, Lee J-Y, Seok H-K. Influence of Ca on the corrosion properties of magnesium for biomaterials. Mater Lett 2008;62(25):4146–8.
[29] Pietak A, Mahoney P, Dias GJ, Staiger MP. Bone-like matrix formation on magnesium and magnesium alloys. J Mater Sci Mater Med 2008;19(1):407–15.
[30] Robert CW. CRC handbook of chemistry and physics. 66th ed.; 1985–1986.
[31] Kokubo T. Formation of biologically active bone-like apatite on metals and polymers by a biomimetic process. Thermochim Acta 1996;280/281:479–90.
[32] ISO-10993e5: biological evaluation of medical devices e part 5: tests for cytotoxicity: in vitro methods. Arlington, VA: ANSI/AAMI; 1999.
[33] Zhang S, Li J, Song Y, Zhao C, Zhang X, Xie C, et al. In vitro degradation, hemolysis and MC3T3-E1 cell adhesion of biodegradable Mg–Zn alloy. Mater Sci Eng C Biomim Mater Sens Syst 2009;29(6):1907–12.
[34] Xu L, Pan F, Yu G, Yang L, Zhang E, Yang K. In vitro and in vivo evaluation of the surface bioactivity of a calcium phosphate coated magnesium alloy. Biomaterials 2009;30:1512–23.
[35] Witte F, Feyerabend F, Maier P, Fischer J, Störmer M, Blawert C, et al. Biodegradable magnesium-hydroxyapatite metal matrix composites. Biomaterials 2007;28:2163–74.
[36] Zhang E, Yang L, Xu J. Microstructure, mechanical properties and biocorrosion properties of Mg–Si(–Ca) alloy for biomedical application. THERMEC'; 2009. In: International conference on progressing & manufacturing of advanced materials, Biomaterials & Biomedical Applications I – 1st Symposium on degradable metals for biomedical applications.
[37] Witte F, Ulrich H, Rudert M, Willbold E. Biodegradable magnesium scaffolds: part I: appropriate inflammatory response. J Biomed Mater Res 2007;81A:748–56.
[38] Lai JCK, Lai MB, Jandhyam S, Dukhande V, Bushan A, Daniels CK, et al. Exposure to titanium dioxide and other metallic oxide nanoparticles induce cytotoxicity on human neural cells and fibroblasts. Int J Nanomed 2008;3(4):533–45.
[39] Lin W, Xu Y, Huang C-C, Ma Y, Shannon KB, Chen D-R, et al. Toxicity of nano- and micro-sized ZnO particles in human lung epithelial cells. J Nanopart Res 2009;11:25–9.
[40] Nair S, Sasidharan A, Divya Rani VV, Menon D, Nair S, Manzoor K, et al. Role of size scale of ZnO nanoparticles and microparticles on toxicity toward bacteria and osteoblast cancer cells. J Mater Sci Mater Med 2008;. doi:10.1007/s10856-008-3548-5.